



Synthesis, crystal structure, DFT, Hirshfeld Surface and Molecular docking studies of a novel chalcone derivative (E)-3-(2-chlorophenyl)-1-(2-fluoro-4-methoxyphenyl)prop-2-en-1-one

T. K. Madhura^a, B. M. Rajesh^{b*}, K. Chandra Kumar^c, Chandra^d, S. Shubha^b, N Srikantamurthy^e,
B. Sachuthananthan^f

^aDepartment of Education, Mount Carmel College, Autonomous, Bengaluru-560052, Karnataka, India

^{b*}Department of Physics, R V College of Engineering, Bengaluru-560059, Karnataka, India

^cDepartment of Physics, HKBK College of Engineering, Bengaluru-560045, Karnataka, India

^dDepartment of Physics, The National Institute of Engineering (NIE), Mysore-570008, Karnataka, India,

^eDepartment of Chemistry, Vidyavardhaka College of Engineering, Visvesvaraya Technological University, Mysore-570002, Karnataka, India

^fDepartment of Mechanical Engineering, Sree Vidyanikethan Engineering College, Tirupati-517102, Andhra Pradesh, India

*rajeshbm@rvce.edu.in

Abstract:

In the present research work, a novel chalcone derivative (E)-3-(2-chlorophenyl)-1-(2-fluoro-4-methoxyphenyl)prop-2-en-1-one has been synthesized based on Claisen-Schmidt reaction by using aromatic aldehydes and aromatic ketones. A single crystal was obtained by recrystallization using cold ethanol and a gradual evaporation technique. It has been characterized by the single-crystal X-ray diffraction method. The synthesized crystal was found to be a monoclinic lattice with a $P21/c$ space group. In Hirshfeld surface analysis d_{norm} shows that two red spots correspond to C-H...O contacts in hydrogen bonds and the 2D fingerprint highlighting the H...H interaction contributes 32.3% of the overall crystal packing. The optimized geometry of the title compound was obtained using B3LYP level of density functional theory calculation with a 631G(d,p) basis set. The title molecule docked to the active sites of the receptor 1KZN and the best binding confirmation was obtained.

Keywords: Chalcone, Single crystal XRD, Hirshfeld Surface, DFT, Molecular Docking

Introduction:

Chalcones are polyphenolic compounds belonging to the flavonoid family having two benzenoid rings connected by an aliphatic chain having three carbon atoms, α, β -unsaturated

carbonyl group[1–3] as shown in figure 1. Literature survey reveals that chalcones and their derivatives found in various therapeutic fields show diverse pharmacological activities as drug molecules and they showed antimicrobial, antifungal[4] and antitumor activities[5, 6]. Nowadays several chalcones are used for the treatment for cardiovascular diseases[7], viral disorders[8], gastritis, antarthritic, antiulcer[9], amoebicidal, immunosuppressive[10] neurodegenerative diseases[11] and infectious diseases[12]. Chalcone has demonstrated clinical potential as a novel anticancer drug agent. It is expected that the combination of chalcones provides an effective way to develop anticancer therapeutic efficacy[13]. In this work, a sincere effort is made to study the medicinal behaviour of the synthesized sample using various computational methods and the results are discussed.

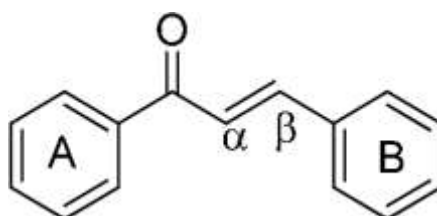


Figure 1: Structure of chalcone.

In this work, the entitled chalcone derivative was synthesised and recrystallised. The crystal structural data were obtained by a single crystal X-ray diffraction experiment using Bruker Smart Apex II Ultra. The theoretical analysis of the sample was done using DFT computational method and the findings are validated with experimental data. Further, the Hirshfeld surface analysis was done for the title molecule and intermolecular interactions were studied and reported. Molecular docking studies were performed using Auto Dock 4.2 software and binding confirmations were discussed and reported.

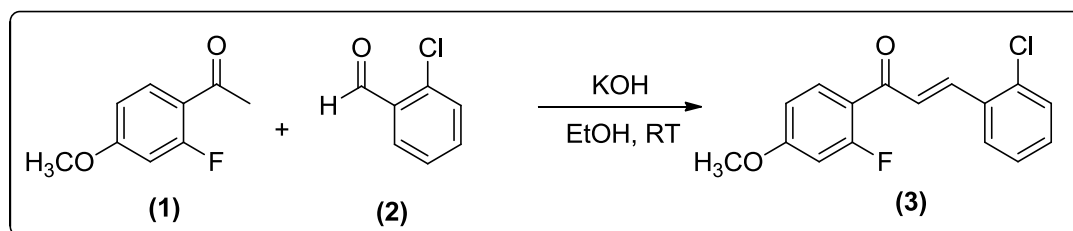
Experimental and Computational Methods

Synthesis of the compound:

A published approach[14] was used to create a chalcone (3), with a few minor alterations, as shown in Scheme 1. In order to carry out the reaction, 5 mmol of 1-(2-fluoro-4-methoxyphenyl)ethanone (1) and 5 mmol of 2-chlorobenzaldehyde (2) were introduced to a flask with a round bottom. Then, after 1.5 hours of constant stirring, 10 mL of 60 % of the KOH solution was progressively added to the mixture. The mixture was agitated once more after the KOH addition for 14 to 16 hours at room temperature. 1.5 mL of 10 % HCl was

added to the reaction mixture after the TLC-tested reaction had finished. The resulting crude product was then filtered via a Buchner filter until the precipitate was obtained. The crude solid was then cleaned with ice-cold water and let to air dry. A single crystal appropriate for X-ray diffraction was obtained by recrystallization using cold ethanol and a gradual evaporation technique.

In this reaction, enolate anions (carbanions) formed from acetophenone derivatives by hydroxide base attract α -hydrogen. β -hydroxy carbonyl intermediates formed from carbanion by attracting carbonyl of benzaldehyde derivatives. This intermediate produced Chalcone under acidic conditions [15].



Scheme 1: Synthesis of chalcone (E)-3-(2-chlorophenyl)-1-(2-fluoro-4-methoxyphenyl)prop-2-en-1-one

X-ray crystallographic details.

The solid state structure of the molecular crystal $C_{16}H_{12}ClF_2NO_2$ was subjected to diffraction using Bruker Kappa Apex II single crystal X-Ray diffractometer equipped with MoK α radiation of wavelength 0.71073\AA at room temperature [16]. The crystal structure obtained from XRD method data was solved using the direct method SHELXS [17]. The structure refinement was performed using SHELXL [18] software package. With anisotropic displacement parameters, nonhydrogen atoms were refined isotropically by including hydrogen atoms in idealised positions. The refined structural data were obtained from the cif file of the title molecule and a summary of the crystal is shown in table 1.

The synthesized crystal was found to be a monoclinic lattice with a $P21/c$ space group. The values of cell edges were found as $a = 15.3830(5)\text{\AA}$, $b = 6.9458(2)\text{\AA}$ and $c = 13.3251(4)\text{\AA}$. The interfacial angles were found as $\alpha = 90^\circ$, $\beta = 102.209(2)^\circ$ and $\gamma = 90^\circ$ confirming the monoclinic formation of the unit cell. The unit cell parameters obtained from the cif file are listed in Table 1. The experimental data of bond lengths and bond angles between the atoms of the molecule are tabulated in Tables 2 and 3 respectively. The linear regression coefficients of

bond lengths (Adjusted $R^2 = 0.992$) and bond angles (Adjusted $R^2 = 0.931$) computed theoretically using DFT are found to be in good agreement with experimental XRD data and shown in Figure 2 & 3 respectively. The small inconsistencies are due to the fact that the theoretical calculations were carried out on an isolated molecule in the gas phase, while the experimental data were acquired in the solid state. The ORTEP of the molecule drawn with 50% thermal ellipsoids is shown in Figure 4. The packing diagram of a unit cell of the molecular crystal viewed along axis A is shown in Figure 5.

The crystallographic data (cif) of the newly synthesized molecule ($C_{16}H_{12}ClFO_2$) have been deposited to the Cambridge Crystallographic Data Centre and assigned deposition number 2182330.

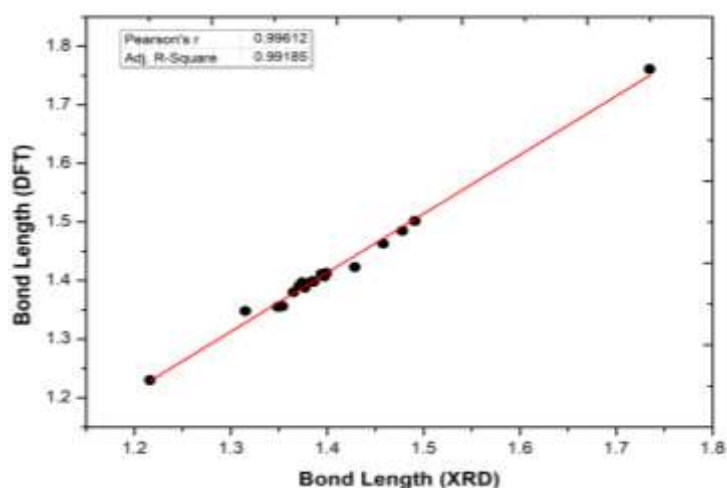


Figure 2: Linear regression coefficient of Bond length between XRD and DFT.

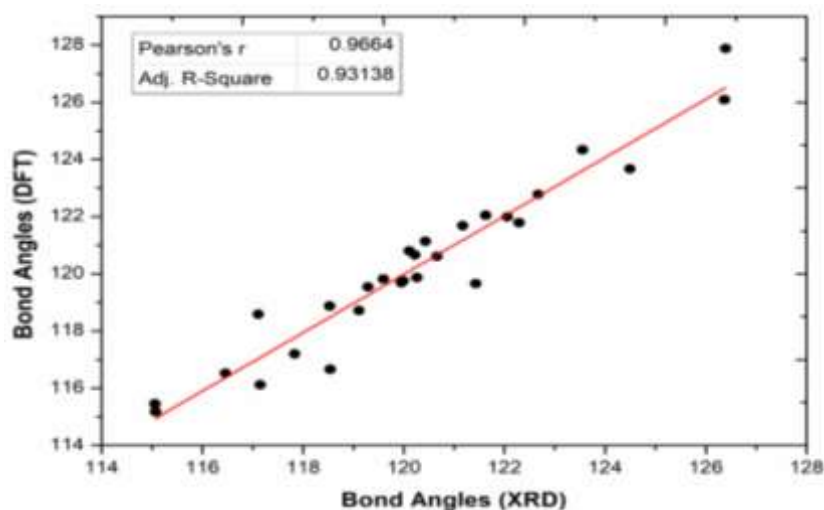


Figure 3: Linear regression coefficient of the Bond angle between XRD and DFT.

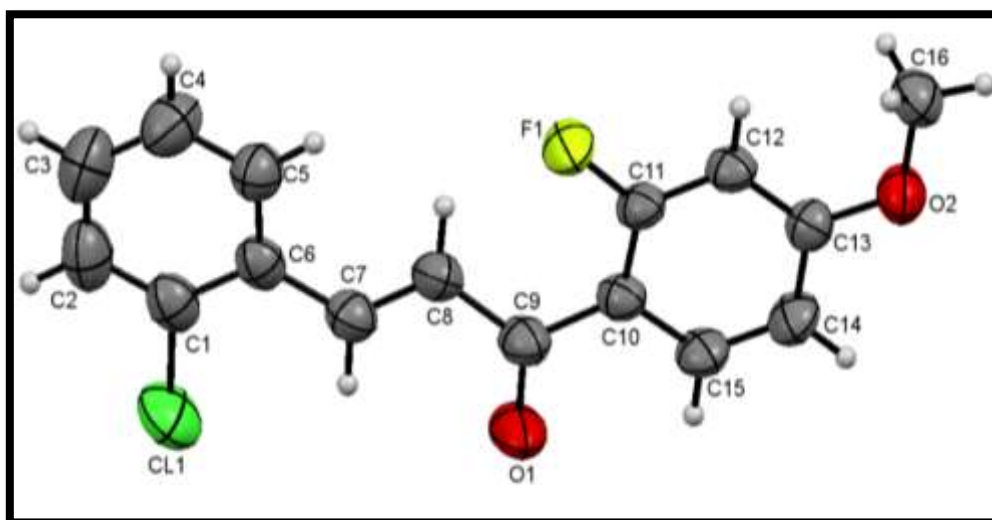


Figure 4: ORTEP diagram of $C_{16}H_{12}ClFO_2$ with thermal ellipsoids drawn at 50% probability.

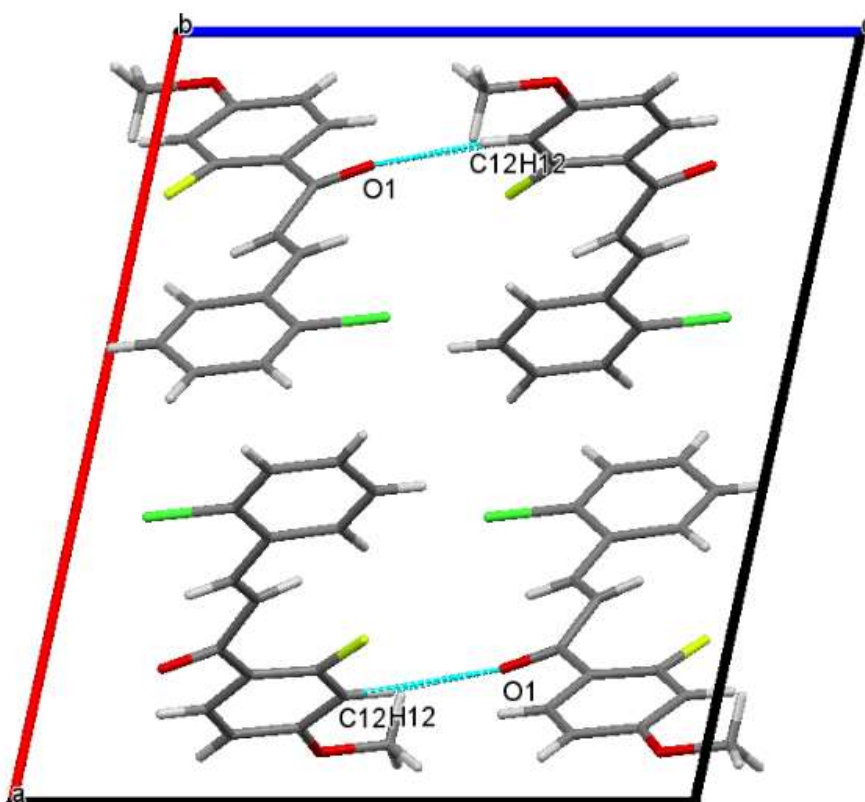


Figure 5: Packing diagram $C_{16}H_{12}ClFO_2$ viewed along the A axis.

Table 1: Crystal structure data

CCDC deposition number	2182330
Structure solution	SHELXT 2014/5
Structure refinement	SHELXL-2016/4
Chemical Formula	C ₁₆ H ₁₂ ClFO ₂
Cell measurement temperature	293(2)
Diffraction radiation wavelength	0.71073 Å
Diffraction radiation type	MoK α
Chemical formula weight	309.71 / g mol ⁻¹
Spacegroup	P 21/c
Space group crystal system	Monoclinic
Cell length "a"	15.3830(5) Å
Cell length "b"	6.9458(2) Å
Cell length "c"	13.3251(4) Å
Cell angle "α"	90°
Cell angle "β"	102.209(2)°
Cell angle "γ"	90°
Cell volume	1391.55(7) Å ³
Cell formula units "Z"	4
Experimental crystal density	1.478 g cm ⁻³
F(000)	636
Experimental absorption coefficient	0.298 μ/mm ⁻¹
Ranges/Indices (hkl)	h: (-20 to +20) k: (-9 to +9) l: (-17 to +17)
Total number of measured reflections	25164
Number of unique reflections	3458
Intense reflections (I > 2σ(I))	2337
Refined parameters	182
θmax	0.999
θmin	1.000
R-factor	0.0680
Weight residual factor for intense reflections wR	0.0424
Goodness of fit on F ²	1.095
su(shift uncertainty) max	0.000
su mean	0.000
Highest difference peak	0.220
deepest hole e/Å ⁻³	-0.212
(1-σ) level	0.039

Table 2: Bond Length

Sl. No	Atom 1	Atom 2	XRD	DFT
1	C11	C1	1.7347(19)	1.761
2	F1	C11	1.3537(16)	1.356
3	O2	C13	1.3489(19)	1.355
4	O2	C16	1.4288(19)	1.423
5	C13	C12	1.386(2)	1.398
6	C13	C14	1.397(2)	1.407
7	C10	C11	1.3846(19)	1.399
8	C10	C15	1.399(2)	1.413
9	C10	C9	1.491(2)	1.502
10	C11	C12	1.371(2)	1.391
11	C15	C14	1.365(2)	1.380
12	C7	C8	1.315(2)	1.348
13	C7	C6	1.458(2)	1.463
14	C9	O1	1.2160(19)	1.230
15	C9	C8	1.478(2)	1.485
16	C6	C1	1.394(2)	1.411
17	C6	C5	1.398(2)	1.411
18	C1	C2	1.374(3)	1.394
19	C5	C4	1.377(3)	1.388
20	C2	C3	1.377(3)	1.393
21	C3	C4	1.374(3)	1.397

Table 3: Bond Angles.

Sl. No	Atom 1	Atom 2	Atom 3	XRD(Å)	DFT(Å)
1	C13	O2	C16	117.11(13)	118.59
2	O2	C13	C12	123.55(14)	124.34
3	O2	C13	C14	117.15(14)	116.12
4	C12	C13	C14	119.29(15)	119.54
5	C11	C10	C15	115.06(14)	115.45
6	C11	C10	C9	126.39(13)	127.88
7	C15	C10	C9	118.54(12)	116.66
8	F1	C11	C12	115.07(12)	115.18
9	F1	C11	C10	120.43(14)	121.14
10	C12	C11	C10	124.49(14)	123.67
11	C11	C12	C13	118.53(13)	118.87
12	C14	C15	C10	122.67(13)	122.78
13	C8	C7	C6	126.37(14)	126.09
14	C15	C14	C13	119.95(14)	119.69
15	O1	C9	C8	120.22(15)	120.66
16	O1	C9	C10	119.11(15)	118.72

17	C8	C9	C10	120.66(12)	120.61
18	C1	C6	C5	116.46(16)	116.52
19	C1	C6	C7	122.29(14)	121.79
20	C5	C6	C7	121.17(15)	121.68
21	C2	C1	C6	122.06(17)	121.99
22	C2	C1	CL1	117.83(15)	117.20
23	C6	C1	CL1	120.11(14)	120.80
24	C7	C8	C9	121.43(14)	119.66
25	C4	C5	C6	121.63(18)	122.05
26	C1	C2	C3	119.99(19)	119.75
27	C4	C3	C2	119.6(2)	119.82
28	C3	C4	C5	120.26(19)	119.87

Computational Methods:

Crystal explorer 21.5 was used to study the Hirshfeld surface analysis which provides important information about a molecule in terms of intermolecular interactions in crystal packing. The 2D fingerprint plot gives an insight into the visualization of inter-atomic contacts and their contributions to a molecule. Gaussian 16 software was used to perform the Density Functional Theory (DFT) calculations. The quantum chemistry calculations were carried out to optimize the organic structure using DFT with a hybrid functional B3LYP/6-31G(d,p) basis set in the gaseous phase. Autodock 4.2 was used to perform molecular docking studies to verify the binding affinity between the ligand and the receptor protein.

Hirshfeld Surface Analysis.

The Hirshfeld Surface (HS) graphical tool is used to visualise and display the intermolecular interactions of the molecular structure in the 3D pictorial form[19]. The HS studies and analysis were carried out using an XRD data input file(cif). The normalized contact distance (d_{norm}) is based on the shortest distance between the nuclei existing external and internal to the surface (d_e & d_i) [20]. The mapping of d_{norm} on HS displays red spots having intermolecular contact distance shorter than Vander Waal's radii. These spots indicate the interconnections involved in the hydrogen bonds[21] and have a negative value of d_{norm} [22]. The contact distances longer than Vander Waal's radii are visible as blue colour in d_{norm} and has a positive value of d_{norm} . The white region represents the interactions having interaction length equal to Vander Waal's radii and it is shown in Figure 6. The Hirshfeld surfaces for the synthesised molecule were generated with standard surface resolution. d_{norm} surfaces were generated over

a fixed scale of colour ranging from -0.3745 to 1.1640 Å. d_i surface value is within 0.8968 to 2.5720 Å, d_e surface is within 0.8943 to 2.5905 Å. The shape index mapping is done in the colour range -1.0000 to 1.0000 Å, for curvedness -4.0000 to 4.0000 Å and the fragment patch 0.0000 to 16.0000 Å [23].

The d_{norm} shows two red spots corresponding to C-H...O contacts in hydrogen bonds and the bond length between H-O has 2.117 Å shown in Figure 6. The calculated volume inside the Hirshfeld surface is 341.14 Å³ in the area of 322.53 Å² with globularity (G) 0.732 as well as asphericity (Ω) 0.352 . Globularity for the sphere is 1 and increasingly less than one as the molecular surface becomes more structured so that the titled molecule structure is close to the sphere. G and Ω provide significant information about the shapes of molecules in crystals [24].

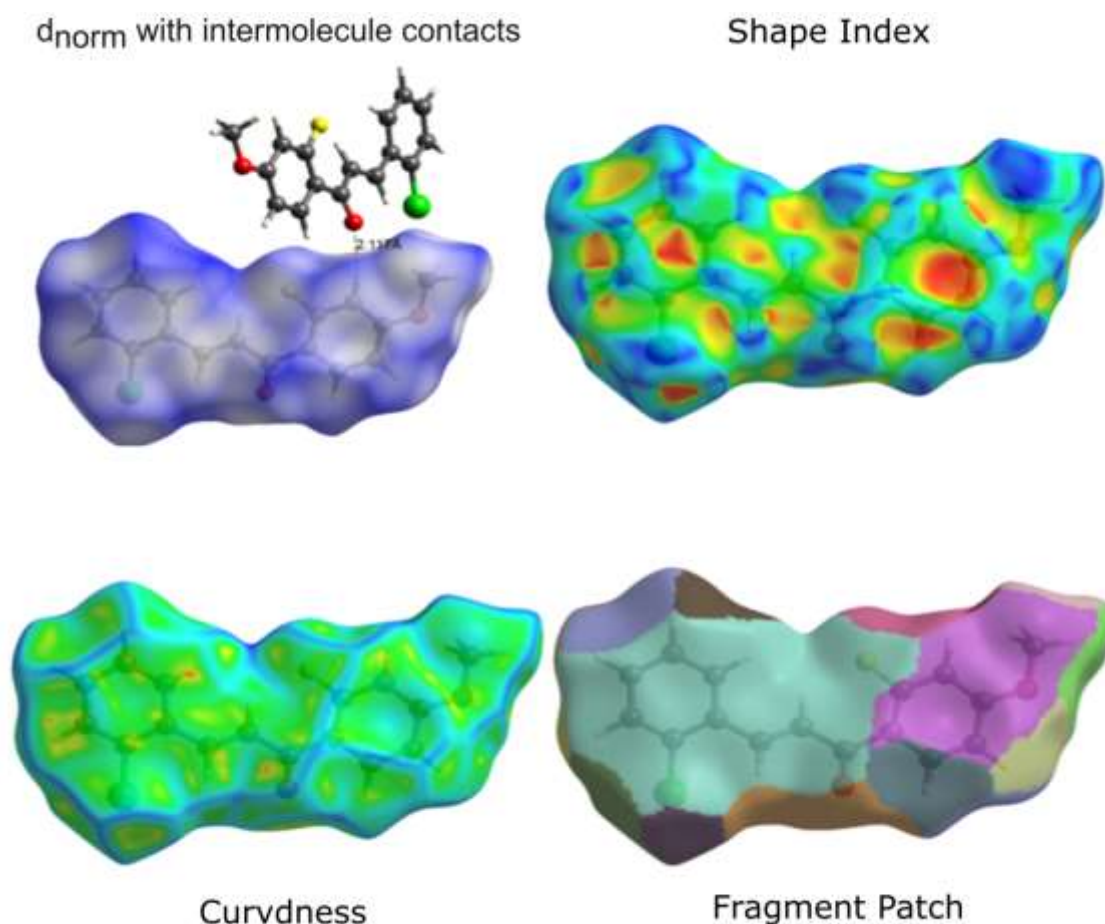


Figure 6: Interatomic molecule interactions mapped on Hirshfeld surface of $C_{16}H_{12}ClFO_2$

The shape index is a qualitative measurement (-1 to 1 a.u.) of the shape of the molecule represented by a complimentary map with bumps and hollows. The blue bump represents

donor electro molecular interactions having an index >1 and the red hallow represents the acceptor of electro molecular interactions having an index <1 [20, 25]. The red and blue adjacent triangles visible in the shape index show the possibility of π - π stacking interactions between the molecules as shown in figure 6. Curvedness ranging from -4.0000\AA to 4.0000\AA shown in Figure 6 displays the local curvature of the surface as relatively flat regions in green colour and edge regions in blue colour which allows to identify the characteristic packing modes of the molecule [26]. They show intermolecular complimentary areas in different colours [22]. Blue edges appearing in between two flat patches shows π - π stacking interactions figure 6.

2-D fingerprint

The 2D fingerprint plot from the Hirshfeld surface represents a unique way of summarizing the intermolecular interactions in the crystal. These plots are generated to identify and measure the intermolecular interactions within the crystal which reveals the minor and major contributors in crystal packing [27]. These plots are resultant of a combination of d_e & d_i and quantify every type of intermolecular interactions present in the molecules [26] and displays as shown in figure 7. It provides a visual summary of the frequency of each combination of d_e and d_i across the surface of a molecule and also the relative area of the surface analogous to each kind of interaction. In a 2D plot, the upper spike having $d_e > d_i$ is linked to the donor hydrogen bond and the lower spike $d_e < d_i$ is linked to the acceptor hydrogen bond [23, 28].

The 2D fingerprint plot highlights the H...H interactions contributing 32.3% of the overall crystal packing which has a large hydrogen content of the molecule with the tip at 2.1\AA , H...C interaction contributes 22.1% having a pair of wings with edges at $d_e + d_i \approx 2.8\text{\AA}$, H...O interactions contributes 12.4% having a pair of spikes with tips at $d_e + d_i \approx 2.1\text{\AA}$. H...Cl interactions contribute 11.9 % having a pair of wings with edges at $d_e + d_i \approx 3.1\text{\AA}$ [20]. These interactions are the primary contributors to the intermolecular stabilization in the crystal as shown in figure 7.

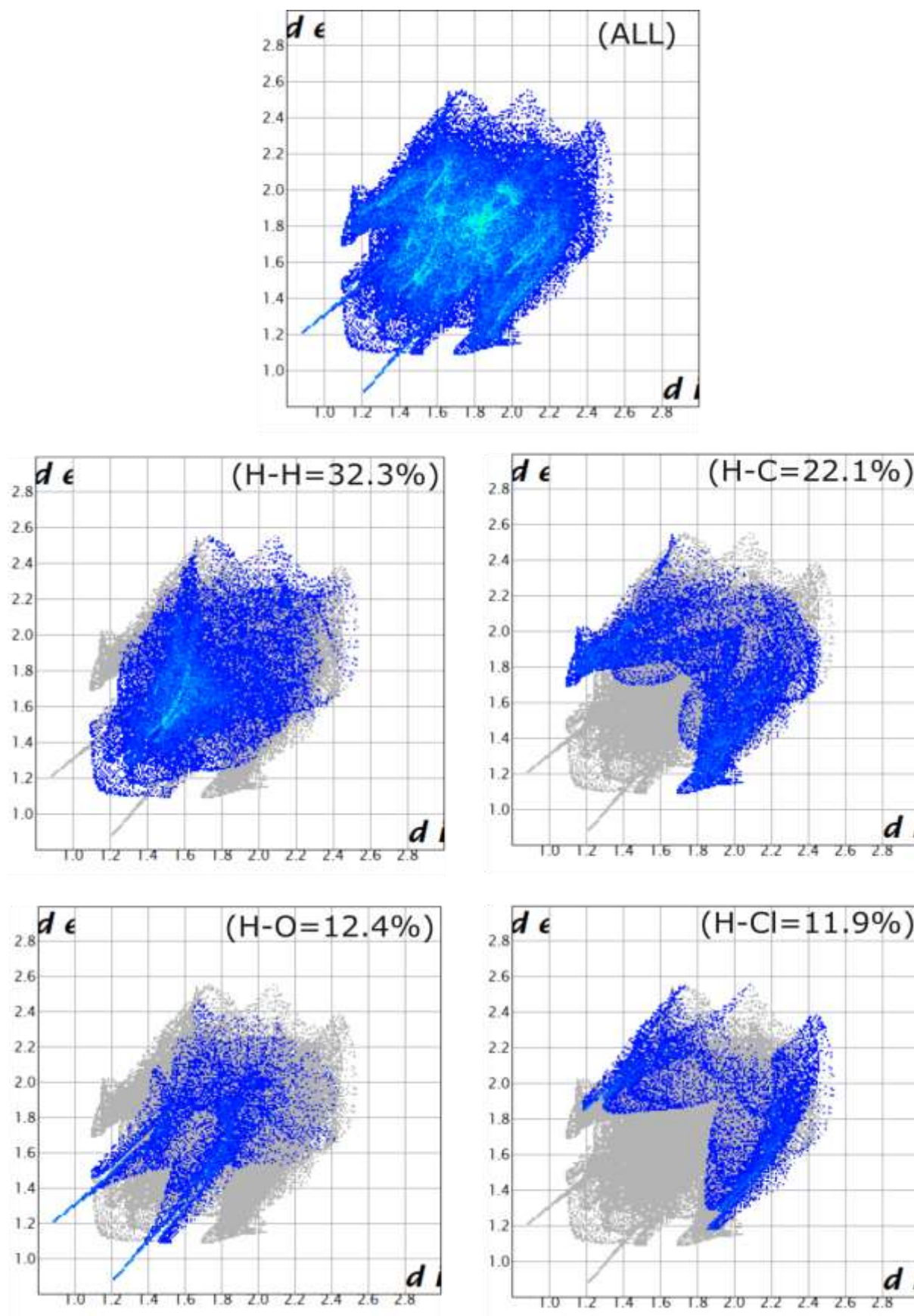


Figure 7: 2D fingerprint plot of $C_{16}H_{12}ClFO_2$

Molecular Docking Studies

The molecular docking simulations were performed using Autodock 4.2. and binding confirmations were visualized [29]. Lamarckian Genetic Algorithm (LGA) computational method is used for optimising the best binding orientations of the ligand molecule with molecular target [30]. The three-dimensional protein (PDB Code: 1KZN) is obtained from the RSCB protein data bank and used as a docking receptor. The intermolecular complex structure formed at best fit is visualised. In this work, the title molecule docked to the active sites of the receptor 1KZN and the best binding confirmation was obtained [31]. The docking results were graded as per the inhibition constant, binding affinity [29] and vdW + Hbond + desolv which are 7.59, -0.35 (kcal/mol) and -8.37 respectively. The compound has a minimum binding energy of -6.98 kJ/mol with 1KZN emerged as the most promising for forming stable complexes. A hydrogen bond interaction was seen between the molecule and the active site of the amino acid Gly77 with a bond length of 2.726 Å as shown in figure 9. The details of docked score results are given in Table 4 and figure 8 (a&b) shows molecule wrapped by active site amino acid residues at the active site pocket regions.

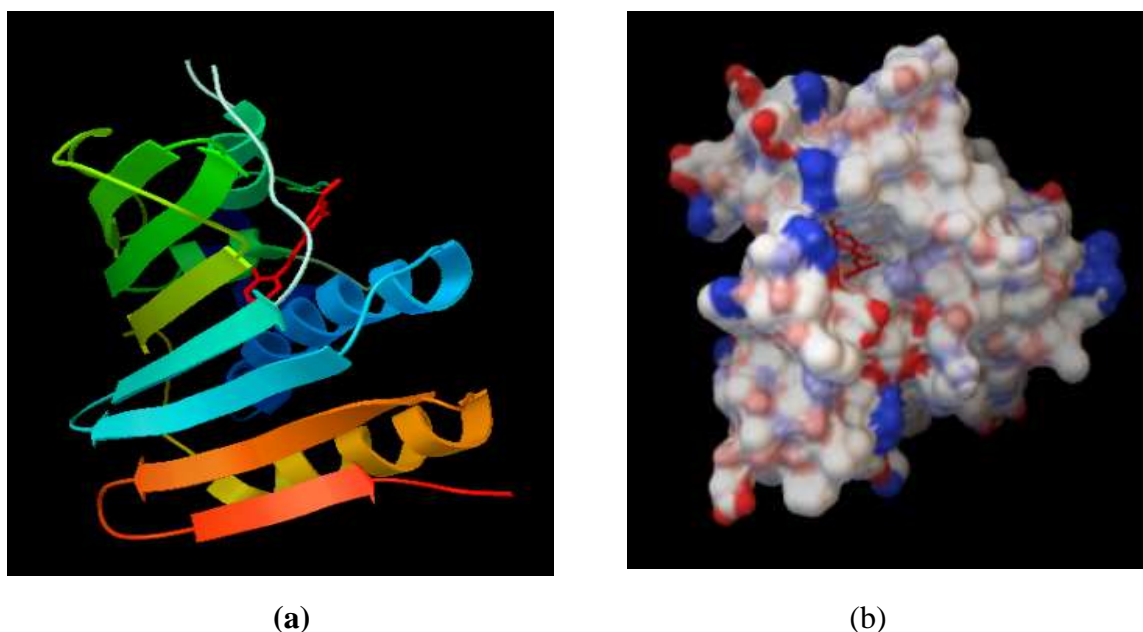


Figure 8 (a&b): Docking and Enfolding of molecule $C_{16}H_{12}ClFO_2$ in the active site pocket of 1KZN

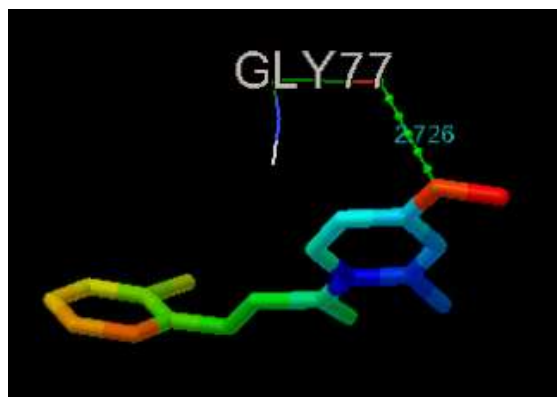


Figure 9: A hydrogen bond interaction between the molecule and the active site of the amino acid Gly77.

Table 4: The dock results of the ligand (NS5) with 1KZN

Compound	Binding Energy (kJ mol ⁻¹)	Ligand Efficiency	Inhibition Constant	vdW+H-bond+desolv energy	No. of H-bonds	Bonding residues	Bond Length (Å)
NS5	-6.98	-0.35	7.59	-8.37	1	1KZN:A:GLY77:O	2.726

Density Functional Theory:

Frontier Molecular Orbital's

In quantum chemistry, understanding of the synthesized molecules in terms of chemical and physical properties via the probability of occupation of electrons in the molecular orbital. It helps to conceptualize the chemical bonding and chemical reactivity in terms of the interaction between frontier molecular orbital like the highest energy level occupied and the lowest energy level unoccupied by the electron [32]. The highest occupied molecular orbital (HOMO) is generally termed as electron donating/nucleophilic whereas the lowest unoccupied molecular orbital (LUMO) is termed as electron accepting/electrophilic [33]. The energy difference between the highest occupied (-6.323 eV) and lowest unoccupied molecular orbital (-2.146 eV) is called the energy gap (4.177 eV) is calculated using B3LYP/6-31G(d,p) hybrid functional, the larger value of the energy gap determines the higher stability and less reactivity of the molecule [34] and it is as shown in the figure 10. Global reactivity parameters are listed in the table 5. The electrophilicity index (ω), is calculated based on thermodynamic properties [35]. It acts as an important parameter in

determining the chemical reactivity of a system. Electron transfer between HOMO and LUMO is described by electronic chemical potential (μ) and chemical hardness (η). Compounds with larger values of chemical potential are more reactive. Electronegativity (χ) indicates the measure of electron attraction by an atom.

Table 5: Global reactive parameters and HOMO and LUMO energy values.

HOMO	-6.323 eV
LUMO	-2.145 eV
Energy Gap ($\Delta E = \text{HOMO-LUMO}$)	4.177 eV
Ionization Potential (IP)	6.323 eV
Electron Affinity (A)	2.145 eV
Chemical Potential ($\mu = (\text{HOMO} + \text{LUMO})/2$)	-4.234 eV
Chemical Hardness ($\eta = (\text{LUMO} - \text{HOMO})/2$)	2.089 eV
Electronegativity $\chi = -\mu$	4.234 eV
Electrophilicity $\omega = \mu^2/2\eta$	-4.291 eV
Global softness $\sigma = 1/\eta$	0.479 eV
Maximum electronic charge $\Delta N_{\text{max}} = -\mu/\eta$	2.027 eV

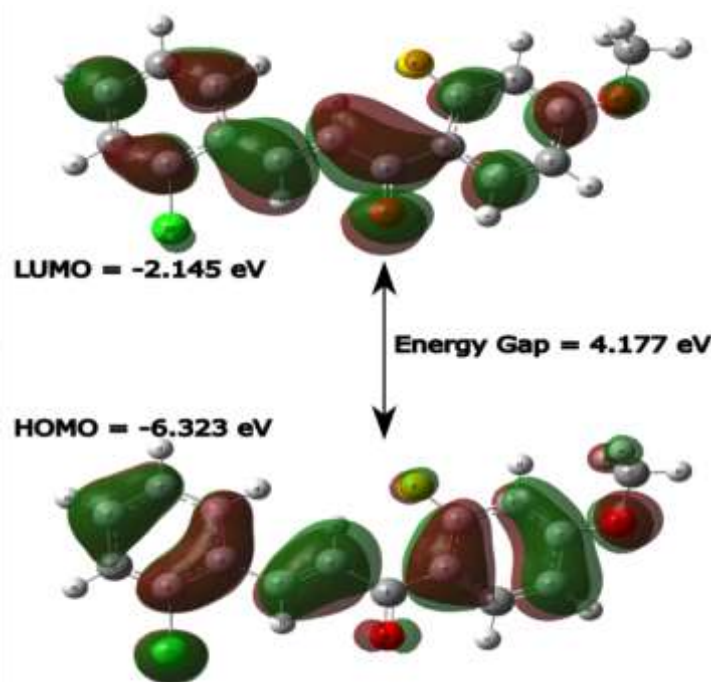


Figure 10: HOMO-LUMO and the Energy gap of the title compound

UV-Vis Spectrum:

The UV-visible spectrum of the title compound was obtained by TD-DFT calculations at the B3LYP/631G(d,p) level of theory [36] and shown in figure 12. Where the optimized structure of the molecule was used as the input file. The epsilon and oscillator strengths of the excited states of a molecule are obtained. Where three major peaks are observed at wavelengths 314.5 nm, 344.7 nm and 363.1 nm due to the excitation of electrons from HOMO to LUMO having energy gaps of 3.33 eV, 3.60 eV and 3.42 eV respectively [37]. λ_{\max} corresponds to 344 nm and can be assigned to $n \rightarrow \pi^*$ transition and may be assigned to the excitation in the aromatic ring and C = O group. The energy gap of 4.12 eV was found from the indirect band gap which was calculated from the tauc's plot as shown in Figure 11 and was comparable to with energy gap obtained from HOMO to LUMO[38].

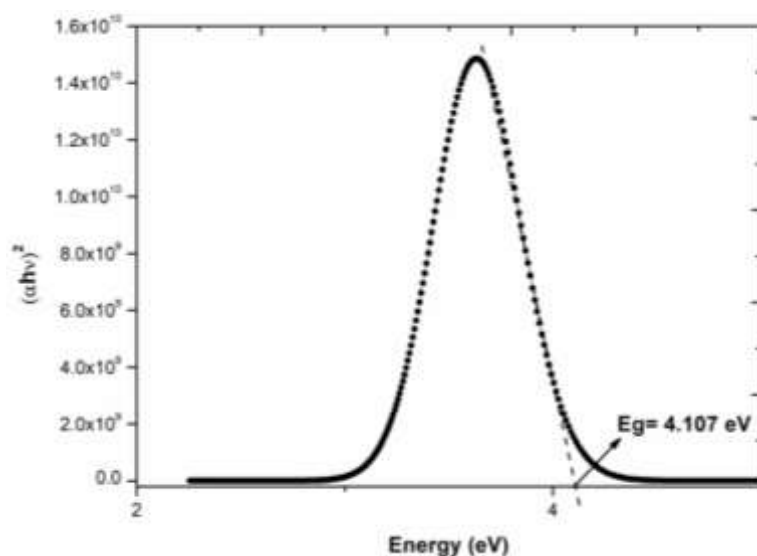


Figure 11: Tauc's Plot of $C_{16}H_{12}ClFO_2$ molecule

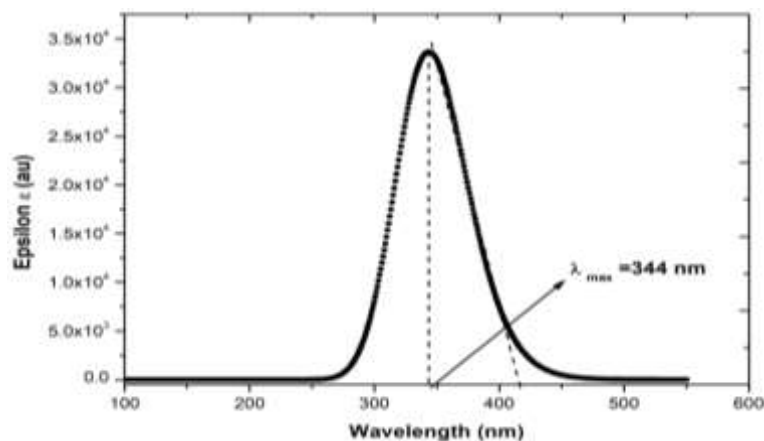


Figure 12: UV-visible spectra of $C_{16}H_{12}ClFO_2$ molecule

Electrostatic Potential Map

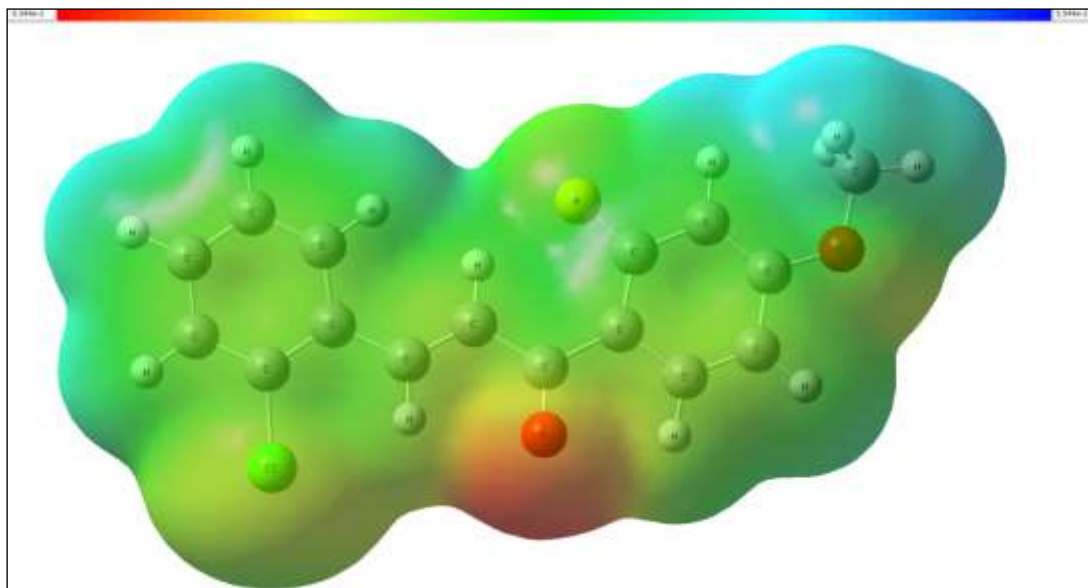


Figure 13: Molecular electrostatic potential map

An electrostatic potential map was generated from the distribution of positive and negative charges in a molecule. It helps to study the intermolecular interactions of molecular systems and to identify the sites for nucleophilic (blue colour) and electrophilic (red colour) attacks [39]. Where electrophilic attack is strong on the oxygen atom and nucleophilic attack is concentrated over the hydrogen atoms is shown in figure 13 [40]. This shows that the most reactive spot of the chalcone molecule is the site containing the oxygen atom.

Conclusions:

In this present research work, we have successfully synthesised and recrystallised the new chalcone derivative. The synthesized crystal was found to be a monoclinic lattice with a *P21/c* space group. The linear regression coefficients of bond lengths (Adjusted R² = 0.992) and bond angles (Adjusted R² = 0.931) computed theoretically using DFT are found to be in good agreement with experimental XRD data. Hirshfeld surface analysis reveals the intermolecular interactions where, d_{norm} shows that two red spots correspond to C-H-O contacts in hydrogen bonds and the 2D fingerprint highlighting the H...H interaction contributing 32.3% of the overall crystal packing. We have also studied the drug ligand interactions and best binding confirmations in molecular docking studies. We have studied the electron density distribution in DFT studies. HOMO/LUMO energy level and quantum parameters are also calculated. The title molecule docked with the active sites of the receptor 1KZN and the best binding confirmation was obtained with an inhibition constant of 7.59.

The compound has a minimum binding energy of -6.98 kJ/mol with 1KZN emerging as the most promising for forming stable complexes. The optimized geometry of the title compound was obtained using B3LYP level of Density functional theory calculation with 631G(d,p) basis set. The energy gap of 4.12 eV was found from the UV-visible spectrum, which was comparable to the energy gap of 4.177 eV obtained from HOMO to LUMO. The larger value of energy gap shows that the higher stability and less reactivity of the molecule. The molecular electrostatic map shows that, electrophilic attack is strong on the oxygen atom and nucleophilic attack is concentrated over the hydrogen atoms.

References:

1. Gomes MN, Muratov EN, Pereira M, et al (2017) Chalcone Derivatives: Promising Starting Points for Drug Design. *Molecules* 22:1210. <https://doi.org/10.3390/molecules22081210>
2. Higgs J, Wasowski C, Marcos A, et al (2019) Chalcone derivatives: synthesis, in vitro and in vivo evaluation of their anti-anxiety, anti-depression and analgesic effects. *Heliyon* 5:e01376. <https://doi.org/10.1016/j.heliyon.2019.e01376>
3. Kamyra G, Rajwinder K, Anju G, Rajendra A (2021) Chalcones: A review on synthesis and pharmacological activities. *J Appl Pharm Sci.* <https://doi.org/10.7324/JAPS.2021.11s101>
4. Ming LS, Jamalis J, Al-Maqtari HM, et al (2017) Synthesis, characterization, antifungal activities and crystal structure of thiophene-based heterocyclic chalcones. *Chemical Data Collections* 9–10:104–113. <https://doi.org/10.1016/j.cdc.2017.04.004>
5. Boumendjel A, Ronot X, Boutonnat J (2009) Chalcones Derivatives Acting as Cell Cycle Blockers: Potential Anti Cancer Drugs? *Current Drug Targets* 10:363–371
6. Zainuri DA, Arshad S, Khalib NC, et al (2017) Synthesis, XRD crystal structure, spectroscopic characterization (FT-IR, ¹H and ¹³C NMR), DFT studies, chemical reactivity and bond dissociation energy studies using molecular dynamics simulations and evaluation of antimicrobial and antioxidant activities of a novel chalcone derivative, (E)-1-(4-bromophenyl)-3-(4-iodophenyl)prop-2-en-1-one. *Journal of Molecular Structure* 1128:520–533. <https://doi.org/10.1016/j.molstruc.2016.09.022>

7. Mahapatra DK, Bharti SK (2016) Therapeutic potential of chalcones as cardiovascular agents. *Life Sciences* 148:154–172. <https://doi.org/10.1016/j.lfs.2016.02.048>
8. Elkhalfa D, Al-Hashimi I, Al Moustafa A-E, Khalil A (2021) A comprehensive review on the antiviral activities of chalcones. *Journal of Drug Targeting* 29:403–419. <https://doi.org/10.1080/1061186X.2020.1853759>
9. Das B, Samanta S, Burle S, Behera PC (2015) Chalcone as potent molecule: anti-inflammatory, antiarthritic, antioxidant and anti-ulcer a review. *IJPR* 7:1–8
10. V Y, T K, D S, et al (2013) A review on Chalcones and its importance. *PharmaTutor* 1:54–59
11. Królicka E, Kieć-Kononowicz K, Łażewska D (2022) Chalcones as Potential Ligands for the Treatment of Parkinson's Disease. *Pharmaceuticals* 15:847. <https://doi.org/10.3390/ph15070847>
12. Liu W, He M, Li Y, et al (2022) A review on synthetic chalcone derivatives as tubulin polymerisation inhibitors. *Journal of Enzyme Inhibition and Medicinal Chemistry* 37:9–38. <https://doi.org/10.1080/14756366.2021.1976772>
13. Ouyang Y, Li J, Chen X, et al (2021) Chalcone Derivatives: Role in Anticancer Therapy. *Biomolecules* 11:894. <https://doi.org/10.3390/biom11060894>
14. Ismiyanto SMCA (2001) Synthesis of Chalcone and Flavanone Compound Using Raw Mataerial of Acetophenone and Benzaldehyde Derivative = Sistem senyawa Kalkon dan Flavanon Menggunakan Bahan Dasar Senyawa Turunan Asetofenon ... <https://www.semanticscholar.org/paper/Synthesis-of-Chalcone-and-Flavanone-Compound-Using-Ismiyarto/ba601a18cfd49242f3fe6d165ba7e963330c534d>. Accessed 30 Oct 2022
15. Enchev V, Mehandzhiyski AY (2017) Computational insight on the chalcone formation mechanism by the Claisen–Schmidt reaction. *International Journal of Quantum Chemistry* 117:e25365. <https://doi.org/10.1002/qua.25365>
16. brukera2 user manual.pdf

17. Aguiar ASN, Queiroz JE, Firmino PP, et al (2020) Synthesis, characterization, and computational study of a new heteroaryl chalcone. *J Mol Model* 26:243. <https://doi.org/10.1007/s00894-020-04506-1>
18. A. Spackman M, Jayatilaka D (2009) Hirshfeld surface analysis. *CrystEngComm* 11:19–32. <https://doi.org/10.1039/B818330A>
19. D H, Bairy R, A J, et al (2021) Structural, photoluminescence, physical, optical limiting, and hirshfeld surface analysis of polymorphic chlorophenyl organic chalcone derivative for optoelectronic applications. *Journal of Molecular Structure* 1232:130053. <https://doi.org/10.1016/j.molstruc.2021.130053>
20. Kamath L, Menezes AP, Bairy R, et al (2021) Hirshfeld surface analysis, enrichment ratio, energy frameworks and third-order nonlinear optical studies of a hydrazone derivative for optical limiting applications. *Journal of Molecular Structure* 1245:131019. <https://doi.org/10.1016/j.molstruc.2021.131019>
21. Ternavisk RR, Camargo AJ, Machado FBC, et al (2014) Synthesis, characterization, and computational study of a new dimethoxy-chalcone. *J Mol Model* 20:2526. <https://doi.org/10.1007/s00894-014-2526-8>
22. Fatima A, Pooja Km, Savita S, et al (2021) Quantum Chemical, experimental spectroscopic, Hirshfeld surface and molecular docking studies of the anti-microbial drug Sulfathiazole. *Journal of Molecular Structure* 1245:131118. <https://doi.org/10.1016/j.molstruc.2021.131118>
23. Baylan D, Sagdinc SG (2019) Hirshfeld surface analysis of diclofenac acid. *AIP Conference Proceedings* 2178:030029. <https://doi.org/10.1063/1.5135427>
24. Chandini KM, Nagesh Khadri MJ, Amoghavarsha N, et al (2022) Synthesis, crystal structure, Hirshfeld surface analysis, energy frameworks and computational studies of Schiff base derivative. *Heliyon* 8:e10047. <https://doi.org/10.1016/j.heliyon.2022.e10047>
25. Tan SL, Jotani MM, Tiekink ERT (2019) Utilizing Hirshfeld surface calculations, non-covalent inter-action (NCI) plots and the calculation of inter-action energies in the

- analysis of mol-ecular packing. *Acta Cryst E* 75:308–318. <https://doi.org/10.1107/S2056989019001129>
26. Valverde C, Castro AN, Rodrigues RFN, et al (2019) Hyperpolarizability studies and Hirshfeld surface analysis of two heterocyclic chalcones. *J Mol Model* 25:324. <https://doi.org/10.1007/s00894-019-4209-y>
 27. Gomes LR, Low JN, Wardell JL (2021) Crystal structures, Hirshfeld surface analysis and PIXEL calculations of two chalcone derivatives, containing isopropoxy substituents: Importance of dispersion energy. *Journal of Molecular Structure* 1237:130354. <https://doi.org/10.1016/j.molstruc.2021.130354>
 28. McKinnon JJ, Spackman MA, Mitchell AS (2004) Novel tools for visualizing and exploring intermol-ecular interactions in molecular crystals. *Acta Cryst B* 60:627–668. <https://doi.org/10.1107/S0108768104020300>
 29. Yalcin G, Burmaoglu S, Yildiz I, Algul O (2018) Molecular docking studies on fluoro-substituted chalcones as potential DprE1 enzyme inhibitors. *Journal of Molecular Structure* 1164:50–56. <https://doi.org/10.1016/j.molstruc.2018.02.087>
 30. Fuhrmann J, Rurainski A, Lenhof H-P, Neumann D (2010) A new Lamarckian genetic algorithm for flexible ligand-receptor docking. *Journal of Computational Chemistry* 31:1911–1918. <https://doi.org/10.1002/jcc.21478>
 31. Vijesh AM, Isloor AM, Telkar S, et al (2013) Molecular docking studies of some new imidazole derivatives for antimicrobial properties. *Arabian Journal of Chemistry* 6:197–204. <https://doi.org/10.1016/j.arabjc.2011.10.007>
 32. Yu J, Su NQ, Yang W (2022) Describing Chemical Reactivity with Frontier Molecular Orbitals. *JACS Au* 2:1383–1394. <https://doi.org/10.1021/jacsau.2c00085>
 33. Zhuo L-G, Liao W, Yu Z-X (2012) A Frontier Molecular Orbital Theory Approach to Understanding the Mayr Equation and to Quantifying Nucleophilicity and Electrophilicity by Using HOMO and LUMO Energies. *Asian Journal of Organic Chemistry* 1:336–345. <https://doi.org/10.1002/ajoc.201200103>

34. Miar M, Shiroudi A, Pourshamsian K, et al (2021) Theoretical investigations on the HOMO–LUMO gap and global reactivity descriptor studies, natural bond orbital, and nucleus-independent chemical shifts analyses of 3-phenylbenzo[d]thiazole-2(3H)-imine and its para-substituted derivatives: Solvent and substituent effects. *Journal of Chemical Research* 45:147–158. <https://doi.org/10.1177/1747519820932091>
35. Parr RG, Szentpály L v., Liu S (1999) Electrophilicity Index. *J Am Chem Soc* 121:1922–1924. <https://doi.org/10.1021/ja983494x>
36. Castro ME, Percino MJ, Chapela VM, et al (2013) Comparative theoretical study of the UV/Vis absorption spectra of styrylpyridine compounds using TD-DFT calculations. *J Mol Model* 19:2015–2026. <https://doi.org/10.1007/s00894-012-1602-1>
37. Costa JCS, Taveira RJS, Lima CFRAC, et al (2016) Optical band gaps of organic semiconductor materials. *Optical Materials* 58:51–60. <https://doi.org/10.1016/j.optmat.2016.03.041>
38. Xue Y, Mou J, Liu Y, et al (2010) An ab initio simulation of the UV/Visible spectra of substituted chalcones. *Open Chemistry* 8:928–936. <https://doi.org/10.2478/s11532-010-0058-3>
39. Murray JS, Politzer P (2011) The electrostatic potential: an overview. *WIREs Computational Molecular Science* 1:153–163. <https://doi.org/10.1002/wcms.19>
40. Zaini MF, Razak IA, Khairul WM, Arshad S (2020) Structural, Hirshfeld and DFT studies of conjugated D– π –A carbazole chalcone crystal. *Acta Crystallogr E Crystallogr Commun* 76:387–391. <https://doi.org/10.1107/S2056989020002054>